In Situ Transmission Electron Microscopy Study of Electrochemical Lithiation and Delithiation Cycling of the Conversion Anode RuO_2

Keith E. Gregorczyk,[†,‡,⊥] Yang Liu,[§,⊥,*] John P. Sullivan,[§] and Gary W. Rubloff[†,‡,*]

[†]Department of Materials Science and Engineering and [‡]Institute for Systems Research, University of Maryland, College Park, Maryland 20742, United States and [§]Center for Integrated Nanotechnologies, Sandia National Laboratories, Albuquerque, New Mexico 87185, United States. [⊥]These authors contributed equally to the research and writing of this paper.

ABSTRACT Conversion-type electrodes represent a broad class of materials with a new Li^+ reactivity concept. Of these materials, RuO_2 can be considered a model material due to its metallic-like conductivity and its high theoretical capacity of 806 mAh/g. In this paper, we use *in situ* transmission electron microscopy to study the reaction between single-crystal RuO_2 nanowires and Li^+. We show that a large volume expansion of 95% occurs after lithiation, 26% of which is irreversible after delithiation. Significant surface roughening and lithium embrittlement are also present. Furthermore, we show that the initial reaction from crystalline RuO_2 to the fully lithiated mixed phase of Ru/Li_2O is not fully reversible, passing through an intermediate phase of Li_xRuO_2. In subsequent cycles, the phase transitions are between amorphous RuO_2 in the delithiated state and a nanostructured network of Ru/Li_2O in the fully lithiated phase.

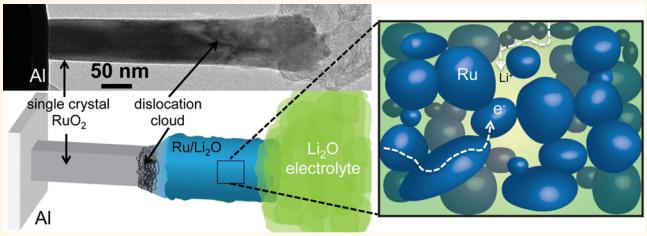

KEYWORDS: *in situ* transmission electron microscopy · energy storage · ruthenium dioxide · conversion electrode

In *situ* transmission electron microscopy (TEM) studies have become a rapid way to screen and understand lithiation behaviors and reaction chemistries during charging/discharging of lithium ion battery (LIB) materials and have recently led to major advances in the characterization of mechanical and chemical changes in these complex systems.[1,2] A variety of LIB materials have been studied using several different configurations,[1,2] such as SnO_2,[3−7] Si,[8−13] Ge,[14] Al,[15] carbonaceous materials such as multiwalled carbon nanotubes (MWCNT) and graphene,[16,17] oxides such as ZnO,[18] a variety of coated materials such as a-Si on MWCNT and carbon fibers,[19,20] Si nanoparticles in a carbon matrix,[21] and even a single nanowire battery with a solid-state electrolyte.[22] These results showed that each material behaves differently during the lithiation/delithiation process, although some general trends were observed, including large amounts of stress at the lithiation front—usually indicated by a dense area of dislocations, volume expansion during lithiation, and often embrittlement of the lithiated nanomaterial.[1,2]

Many of these prior studies have focused on materials that alloy with Li and demonstrate high theoretical capacity (*e.g.*, ∼4000 mAh/g for Si) or on next generation carbon materials such as MWCNTs and graphene. Recently, however, there is increased interest in "conversion reaction" materials due to the promise of high capacity, including the possibility of achieving high capacity cathodes—a particular challenge.[23] Materials that are capable of demonstrating true reversible conversion reactions are limited, and there have been very few prior *in situ* TEM studies, with recent work on CuO nanowires and FeF_2 nanoparticles being two exceptions.[24,25]

Materials that undergo a reversible conversion reaction, as opposed to intercalation materials such as C and $LiTiO_2$ and alloy materials such as Si and Sn, have recently been proposed as possible candidates for

* Address correspondence to rubloff@umd.edu, ynliu@sandia.gov.

Received for review May 14, 2013 and accepted June 19, 2013.

Published online June 20, 2013
10.1021/nn402451s

next generation battery electrodes. This conversion reaction has been generalized as follows:

$$M_aX_b + (bn)Li \leftrightarrow aM + bLi_nX \quad (1)$$

where M can be Sn, Ti, V, Cr, Mn, Fe, Co, Ni, Cu, Mo, W, or Ru, and X can be O, S, N, P, or F, and n is the formal oxidation state of X.[23] For example, when RuO_2 is used, the reaction is written $RuO_2 + 4e^- + 4Li^+ \leftrightarrow Ru^0 + 2Li_2O$.[26] Of the conversion oxides, RuO_2 is of particular interest due to its high theoretical specific capacity (806 mAh/g), though it should be noted that the measured capacity of RuO_2 has been reported to be as high as 1130 mAh/g, corresponding to 5.6 mols of Li^+ per mol of RuO_2 due to interfacial ion storage[26] and its low resistivity (36 $\mu\Omega$ cm), making it an ideal material to study reaction mechanisms in conversion-type transition metal oxides.[27] In bulk form, RuO_2 has been studied using commercially available RuO_2 powder, carbon black, graphite, and polyvinylene difluoride, which were mixed together in a weight ratio of 10:1:1:1 and then pasted onto a Ti foil.[26] The first cycle was reported to have a Coulombic efficiency of 98%; however, capacity dropped quickly with limited capacity after three cycles. Follow-up studies to this report used nanosized powders mixed with similar binders.[28−31]

In order to understand the detailed mechanisms of the RuO_2 conversion process, we have undertaken a detailed *in situ* TEM characterization study. We report the first *in situ* observation of electrochemical lithiation−delithiation cycles of the transition metal oxide RuO_2. An intermediate crystal phase Li_xRuO_2 (where x is close to 1) was observed during the first lithiation, consistent with the *ex situ* measurements.[26] From these results, the entire reaction can be written starting with an irreversible reaction from single-crystal RuO_2 through the intermediate phase into a network of Ru/Li_2O. After the first cycle, the reaction becomes partially reversible between amorphous RuO_2 when completely delithiated and a nanoscale network of Ru and Li_2O when fully lithiated. Furthermore, a single RuO_2 nanowire was cycled nine times to study chemical and mechanical degradation during cycling, and these results indicate that, when mechanical stability is maintained, chemical reversibility remains high; however, when the material degrades substantially during cycling, chemical reversibility suffers, and the reaction becomes less reversible due to areas of the Ru/Li_2O network becoming ionically and/or electronically disconnected.

RESULTS AND DISCUSSION

First Cycle Lithiation of a Single-Crystal RuO_2 Nanowire. The results of the nanowire growth process are shown in Figure 1a−d. Large arrays of nanowires of mixed diameter and length can be seen in Figure 1a. The majority of the nanowires have diameters between 30 and 90 nm, and the lengths vary from 1 to several micrometers, though it should be noted that larger particles are also present and can be seen in Figure 1b.

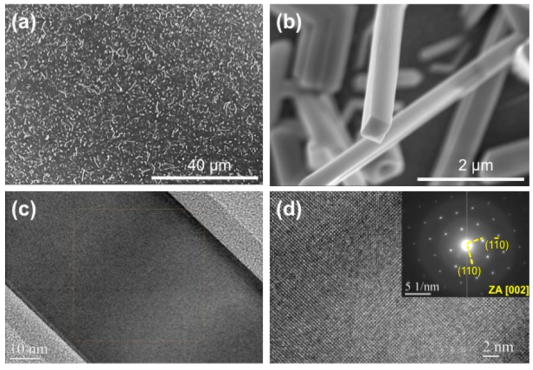

Figure 1. SEM images (a,b) of arrays of RuO_2 nanowires grown through a vapor transport method and TEM images confirming that the wires are single crystal (c,d and inset of d).

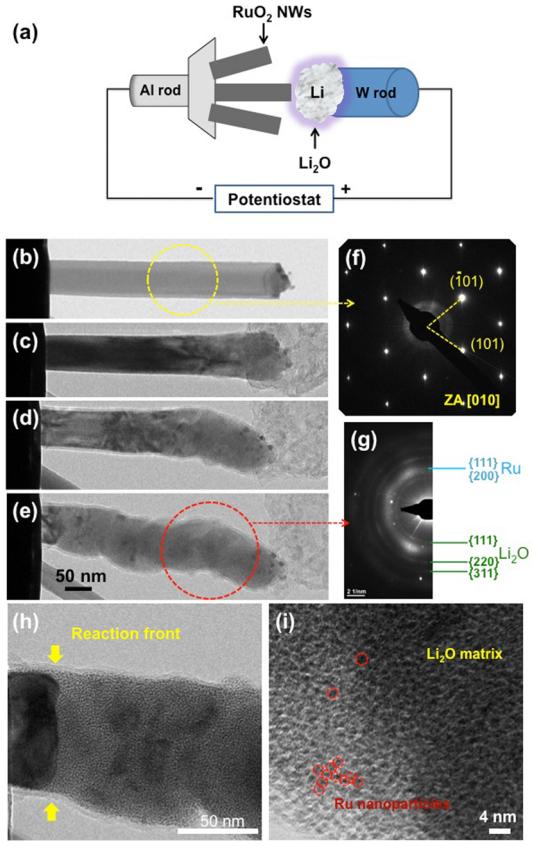

Figure 2. *In situ* TEM setup (a) showing RuO_2 nanowires attached to an Al rod and Li/Li_2O electrode/electrolyte. (b−e) Images of the first cycle lithiation of a single-crystal RuO_2 nanowire showing the large dislocation clouds at the reaction front and dramatic structural changes. (f,g) Corresponding electron diffraction patterns, where it can be seen that the single-crystal RuO_2 becomes Ru and Li_2O. At the reaction front shown in (h), a large cloud of dislocations is present in the RuO_2. After the reaction, a polycrystalline network of Ru/Li_2O can be seen in both (h) and HRTEM image (i). Also see supplemental movie S1 in the Supporting Information.

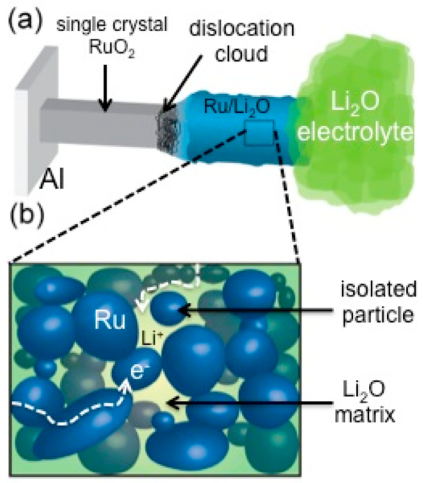

Figure 3. (a) Schematic of the reaction process showing a partially lithiated RuO_2 nanowire and (b) proposed fully reacted Ru/Li_2O showing the facile electron (blue spherical shapes shaded to show depth) and Li-ion (green areas surrounding blue shapes) conduction pathways, as well as an isolated particle—a contribution to irreversibility in the system.

These results compare well to the few reported growth recipes in the literature.[32−34] TEM images show that the nanowires are single-crystal rutile structure, as can been seen in Figure 1c,d and the corresponding inset.

In order to lithiate the nanowires, a −2 V potential was applied to the nanowire against the Li counter electrode. Figure 2b−e and Supporting Information movie S1 show the lithiation of a RuO_2 nanowire. The electron diffraction patterns (EDPs) before and after lithiation are shown in Figure 2f,g along with high-magnification images of the reaction front (Figure 2h) and the reacted zone after the reaction was completed (Figure 2i). A ∼41% increase in the diameter, but little increase in the length, was seen after the first cycle of lithiation, giving a total volume expansion of ∼95%. As the nanowire lithiated, it became a polycrystalline mixture of metallic Ru, Ru^0, and Li_2O as was determined from contrast change in the bright-field images (Figure 2b−e) and the EDPs, which showed the single-crystal rutile structure in Figure 2f and the diffraction rings in Figure 2g changing from single-crystal RuO_2 to polycrystalline Ru/Li_2O. Indexing the EDPs confirms the rutile structure. After lithiation, the {111}, {220}, and {311} Li_2O planes become visible, and the diffuse ring close to Ru {111} and {200} planes indicates the fine structures of Ru nanocrystals.

At the reaction front, as seen in Figure 2h, a large cloud of dislocations is visible, similar to those seen for SnO_2 nanowires, indicating an area of high stress.[3] On the reacted side of the dislocation cloud, a network of Ru/Li_2O is seen as the reaction reaches completion (Figure 2i). The dark contrast spots (examples are circled in red) are Ru nanoparticles, which form a connected network in the Li_2O matrix. The Ru network can serve as a facile conductive path for electrons, while the Li_2O provides a similar path for Li^+. A schematic of this process is shown in Figure 3a,b, showing proposed electron and ion pathways.

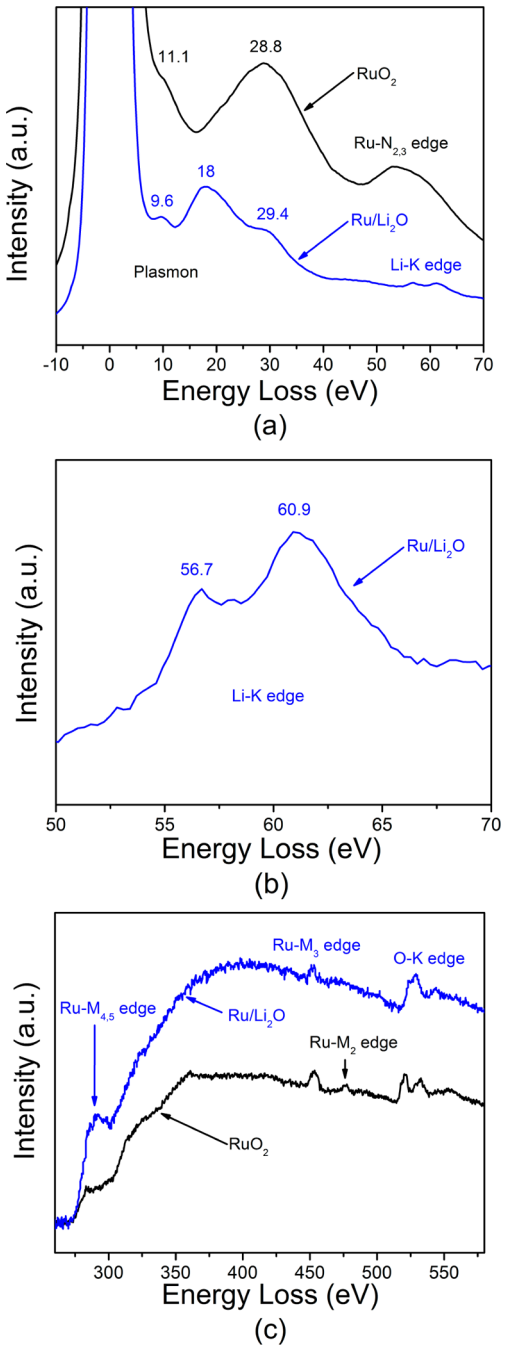

Figure 4. Electron energy loss spectra (EELS) of a single-crystal RuO_2 nanowire (black) and a fully lithiated nanowire which contains a network of Ru/Li_2O. (a) Low loss spectrum for both the lithiated and delithiated nanowires with a magnified view of the Li-K edge in (b). The core loss spectrum is shown in (c).

To confirm the presence of Ru and Li_2O, electron energy loss spectroscopy (EELS) was conducted while the nanowire was in pristine condition and after it was fully lithiated. The results are shown in Figure 4a−c. The low loss EELS spectrum in Figure 4a shows the

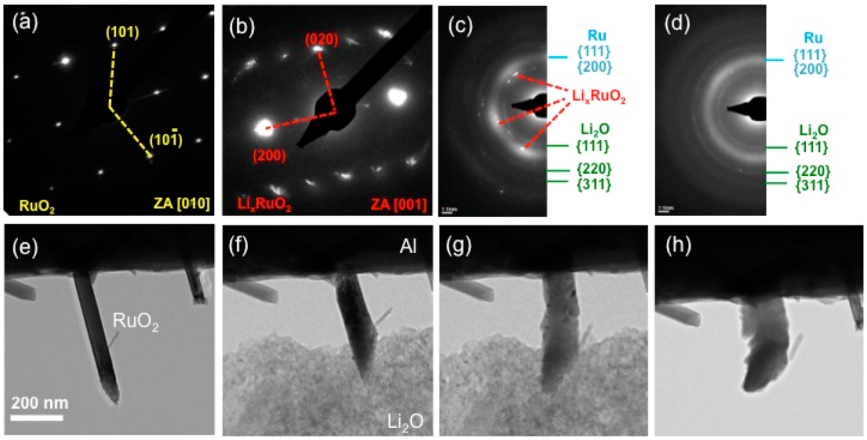

Figure 5. Identification of the intermediate phase Li_xRuO_2. (a−d) Electron diffraction patterns during lithiation with the corresponding bright-field images in (e−h). When a single nanowire is lithiated slowly (−1 V applied), the intermediate phase can be seen (b), which becomes the fully lithated Ru/Li_2O. This intermediate phase is an orthorhombic crystalline phase.

Ru-$N_{2,3}$ edge that, upon lithiation, significantly decreases showing the Li-K edge which can be seen in greater detail in Figure 4b. The Li-K edge appears to be similar to the spectrum expected of Li_2O rather than metallic Li.[35,36] The core loss spectrum can be seen in Figure 4d. After lithiation, the Ru-$M_{4,5}$ edge increased while the Ru $M_{3,2}$ edge decreased.[37,38] There is little work available in the literature that discusses the differences in the EELS spectrum for Ru and RuO_2, making it difficult to quantitatively determine if the changes seen in the Ru-$M_{4,5}$ and Ru-$M_{3,2}$ edges indicate a change from RuO_2 to Ru. However, on the basis of the EDPs in Figure 2 and the Li EELS spectra, we conclude that fully lithiated RuO_2 nanowires consist of Ru/Li_2O.

Intermediate Phase Identification. The existence of an intermediate phase in conversion transition metal oxides has been noted in the literature and confirmed with *ex situ* measurements for RuO_2.[23,26] In order to observe this intermediate phase, the potential was slowly increased from 0 to −1 V and a series of EDPs were taken during lithiation with the results shown in Figure 5a−h. The EDP of a pristine single-crystal RuO_2 nanowire can be seen in Figure 5a, as well as its bright-field image in Figure 5e. When the nanowire was put into contact with the Li_2O and a potential was slowly increased, lithiation began. Figure 5b shows the EDP of the intermediate phase Li_xRuO_2, where x is close to 1, which is an orthorhombic crystal structure. Because the reaction happened so fast and the crystal structures of Li_xRuO_2 were very similar when x is near 1, it was difficult to observe the specific $x = 0.86$ and $x = 1.2$ phases reported using *ex situ* TEM analysis in the literature. It is worth noticing that the diffraction spots in the EDP in Figure 5b became diffuse and curved, indicating the high stress induced distortion of the crystal structure, which was accompanied by the lithium intercalation. Continued lithiation begins the transition from the intermediate phase to the final products Ru/Li_2O (Figure 5c), showing that all three phases exist at the same time. Again, a comparison can be made to the bright-field image (Figure 5g), showing dissipation of the dislocation cloud. Finally, the fully lithiated nanowire EDP can be seen in Figure 5d and its corresponding bright-field image in Figure 5h. The fully lithiated EDP only shows the presence of the Ru {111} and {200} planes and the Li_2O {111}, {220}, and {311} planes, as seen in Figure 2g. These results indicate that direct conversion to the Ru/Li_2O from single-crystal RuO_2 is not energetically favorable but rather requires the intermediate phase discussed here. Finally, continued lithiation brings upon a second phase change where the only two species present are Ru and Li_2O.

Multiple Cycling of a Single Nanowire. Figure 6a−r and Supporting Information supplemental movie S2 show a single RuO_2 NW lithiated and delithiated nine times. To lithiate the nanowire, a −2 V potential was applied, and delithiation was achieved by applying a +4 V potential. Again, a pristine single-crystal nanowire was chosen, as can be seen in Figure 6a,j. The nanowire volume expansion is again seen to be ∼95% after lithiation and is, as expected, composed of Ru/Li_2O, seen in Figure 6b,k. After the first delithiation, however, ∼26% of this volume expansion is irreversible, and the nanowire becomes amorphous RuO_2 (a-RuO_2), as can be seen from the contrast changes between Figure 6a,c and more dramatically in the comparisons of the EDPs seen in Figure 6j,l. While the rutile diffraction pattern is easily identifiable for the pristine RuO_2 wire, after delithiation, all that is visible is an amorphous halo. After the first delithiation, the reaction mechanism proceeds between amorphous RuO_2 and very fine Ru nanoparticles embedded in the polycrystalline Li_2O matrix, as can be seen in the EDPs shown in Figure 6l−r. Specifically, the intermediate phase, Li_xRuO_2, was no longer visible after the first cycle, although it should be noted that an amorphous phase of Li_xRuO_2 may be present but unnoticed due to the speed of the reaction.

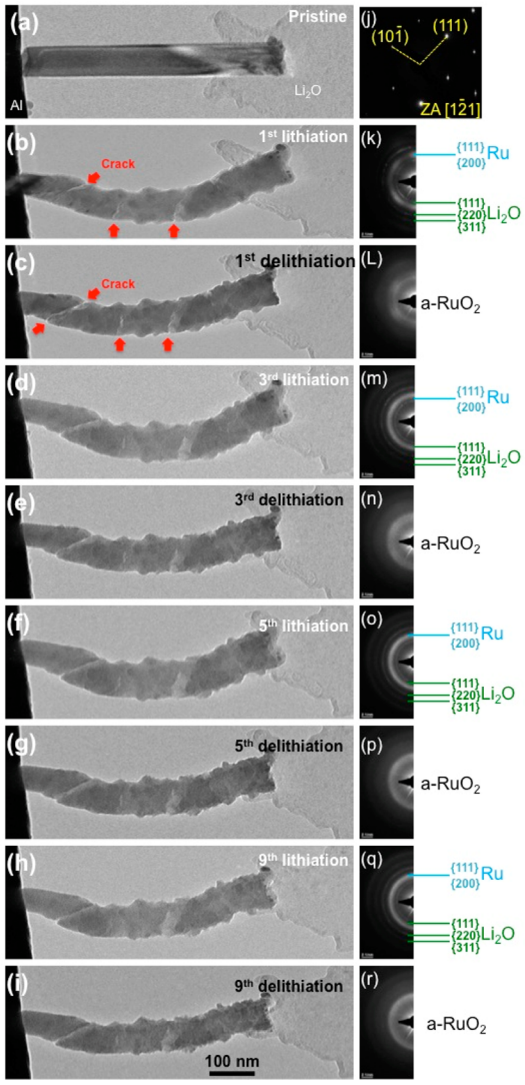

Figure 6. Single RuO_2 nanowire was cycled nine times; see supplemental movie S2 in the Supporting Information. These data show that, after the first cycle, reaction repeatedly goes from a-RuO_2 to a network of Ru/Li_2O.

During the cycling process, mechanical degradation also becomes apparent as the surface of the nanowires is seen to become increasingly rough (Figure 6b–i), and cracks begin to appear (Figure 6b,c), due to lithium embrittlement—a phenomenon seen for several other materials during *in situ* TEM experiments.[1,2] Despite crack formation, electronic and ionic conductivity remain high and the entire structure can be lithiated and delithiated for all nine cycles. All nanowires tested exhibited cracking during the cycling process.

Conclusions. The theoretical reaction mechanism, $RuO_2 + 4e^- + 4Li^+ \leftrightarrow Ru^0 + 2Li_2O$, does not give the full picture of the complicated mutual dependence between mechanical and chemical degradation that takes place during the cycling of RuO_2. From the data shown in Figures 2, 5, and 6, we can confirm that the first lithiation step proceeds as follows:

$$RuO_2(c) + xe^- + xLi^+ \rightarrow Li_xRuO_2(c) \quad (2)$$

Upon continued lithiation, the reaction of the intermediate phase, as detailed in Figure 5, becomes a network of Ru^0 and Li_2O as described here:

$$Li_xRuO_2(c) + (4 - x)e^- + (4 - x)Li^+ \rightarrow Ru^0(c) + 2Li_2O(c) \quad (3)$$

The reaction only becomes reversible after the first cycle and proceeds as follows:

$$a\text{-}RuO_2(a) + 4e^- + 4Li^+ \leftrightarrow Ru^0(c) + 2Li_2O(c) \quad (4)$$

where a-RuO_2 is an amorphous RuO_2 phase, though it may be possible an amorphous phase of Li_xRuO_2 is briefly present during this reaction. The reversibility is highly dependent on the mechanical degradation through maintenance (or loss) of electronic and ionic conductivity. When the nanowires lithiate, significant volume expansion and surface roughening occurs. Furthermore, the lithiation also corresponds to the formation of the Ru/Li_2O matrix, as depicted in Figure 3b. During lithiation, it can be imagined that areas become isolated, preventing complete reversal of this reaction. This behavior was witnessed with a severely mechanically degraded nanowire, shown in Supporting Information Figures S1 and S2 and supplemental movie S3, where HRTEM and HAADF-STEM images were taken after the third delithiation. These images show areas of Ru nanoparticles that were not reacted back to RuO_2; over time, this could significantly reduce the capacity. This phenomenon has been noted as one of the key issues preventing conversion-type materials from becoming more attractive in LIBs.[23]

The results we observed for RuO_2 may also provide insight into the behavior of other conversion-type materials. Less expensive materials such as FeS_2, MnO_2, and TiF_3 may behave in similar ways.[23] It may be possible to cleverly choose a material such that the reaction byproducts are not electrically insulating Li_2O but rather a conductive nitride or phosphide material, for example, thus eliminating the chemical irreversibility.

EXPERIMENTAL SECTION

Single-Crystal RuO_2 Nanowire Growth. RuO_2 nanowires were grown using vapor transport methods available in the literature.[32–34,39] Silicon wafers were coated with a 2 nm layer of gold, used as a catalyst for nanowire growth, and cut into roughly 1 cm by 1 cm pieces. In a commercially available Atomate Nanowire Growth System, which contains a three-zone furnace, a boat of RuO_2 powder (99.99% Aldrich) was placed at one end of the furnace and the Au-coated Si wafers placed downstream of the gas flow at the far end, each in separate zones. The system was then pumped down to 2 Torr

and purged with 100 sccm of Ar (99.99%, Praxair) for 5 min. The RuO_2 powder and Au-coated Si substrates were then ramped to 950 and 670 °C, respectively. Once the temperature was stabilized, O_2 (99.99%, Praxair) was flowed at 200 sccm for 10 h. The pressure was maintained at 2 Torr throughout the reaction. After growth, the RuO_2 nanowires were characterized using a Hitachi SU-70 SEM and a JEOL 2100F TEM.

***In Situ* TEM.** The *in situ* experiments were conducted in a FEI Tecnai F30 TEM. A schematic of the experimental setup is shown in Figure 2a. Li metal was scratched off a newly cut surface of bulk Li with a tungsten (W) rod in a helium-filled glovebox (H_2O and O_2 concentrations below 1 ppm) to serve as the counter electrode and Li source. An aluminum rod was dragged across the surface where the RuO_2 nanowires were grown, resulting in attachment of the nanowires to the aluminum by electrostatic and van der Waals forces. The two electrodes were then mounted onto a Nanofactory TEM-scanning tunneling microscope (STM) holder, which was placed into a plastic bag and sealed in the dry helium environment. During the loading process, the Li was briefly exposed, 2−5 s, to air, forming a native Li_2O layer which served as a solid-state electrolyte. Once the samples were loaded into the TEM, contact was made between the RuO_2 NW and Li_2O through *in situ* nanomanipulation using the STM holder. After contact, an externally controlled fixed potential was applied on the RuO_2 NW against the Li counter electrode to initiate the lithiation and delithiation.

Conflict of Interest: The authors declare no competing financial interest.

Acknowledgment. This work has been supported by Nanostructures for Electrical Energy Storage (NEES), an Energy Frontier Research Center funded by the U.S. Department of Energy, Office of Science, Office of Basic Energy Sciences under Award Number DESC0001160. K.G. was partially supported by the L-3 Communications fellowship. The Laboratory Directed Research and Development (LDRD) program at Sandia National Laboratories (SNL) supported the development and fabrication of the platform used for the nanowire TEM studies. The work was performed in part with the TEM capability supported by the Center for Integrated Nanotechnologies (CINT), an Office of Science User Facility operated for the U.S. Department of Energy (DOE) Office of Science. Sandia National Laboratories is a multiprogram laboratory managed and operated by Sandia Corporation, a wholly owned subsidiary of Lockheed Martin Corporation, for the U.S. Department of Energy's National Nuclear Security Administration under contract DE-AC04-94AL85000.

Supporting Information Available: Movies showing the charging and discharging of single nanowires displayed in Figure 2 and Figure 6, as well as a movie of a severely damaged nanowire. Further information concerning severely damaged wires can be found in the supplementary pdf. This material is available free of charge *via* the Internet at http://pubs.acs.org.

REFERENCES AND NOTES

1. Liu, X. H.; Liu, Y.; Kushima, A.; Zhang, S. L.; Zhu, T.; Li, J.; Huang, J. Y. *In Situ* TEM Experiments of Electrochemical Lithiation and Delithiation of Individual Nanostructures. *Adv. Energy Mater.* **2012**, *2*, 722–741.
2. Liu, X. H.; Huang, J. Y. *In Situ* TEM Electrochemistry of Anode Materials in Lithium Ion Batteries. *Energy Environ. Sci.* **2011**, *4*, 3844–3860.
3. Huang, J. Y.; Zhong, L.; Wang, C. M.; Sullivan, J. P.; Xu, W.; Zhang, L. Q.; Mao, S. X.; Hudak, N. S.; Liu, X. H.; Subramanian, A.; *et al. In Situ* Observation of the Electrochemical Lithiation of a Single SnO_2 Nanowire Electrode. *Science* **2010**, *330*, 1515–1520.
4. Zhong, L.; Liu, X. H.; Wang, G. F.; Mao, S. X.; Huang, J. Y. Multiple-Stripe Lithiation Mechanism of Individual SnO_2 Nanowires in a Flooding Geometry. *Phys. Rev. Lett.* **2011**, 106.
5. Zhang, L. Q.; Liu, X. H.; Perng, Y. C.; Cho, J.; Chang, J. P.; Mao, S. X.; Ye, Z. Z.; Huang, J. Y. Direct Observation of Sn Crystal Growth during the Lithiation and Delithiation Processes of SnO_2 Nanowires. *Micron* **2012**, *43*, 1127–1133.
6. Wang, C. M.; Xu, W.; Liu, J.; Zhang, J. G.; Saraf, L. V.; Arey, B. W.; Choi, D. W.; Yang, Z. G.; Xiao, J.; Thevuthasan, S.; *et al. In Situ* Transmission Electron Microscopy Observation of Microstructure and Phase Evolution in a SnO_2 Nanowire during Lithium Intercalation. *Nano Lett.* **2011**, *11*, 1874–1880.
7. Zhang, L. Q.; Liu, X. H.; Liu, Y.; Huang, S.; Zhu, T.; Gui, L. J.; Mao, S. X.; Ye, Z. Z.; Wang, C. M.; Sullivan, J. P.; *et al.* Controlling the Lithiation-Induced Strain and Charging Rate in Nanowire Electrodes by Coating. *ACS Nano* **2011**, *5*, 4800–4809.
8. Liu, X. H.; Wang, J. W.; Huang, S.; Fan, F. F.; Huang, X.; Liu, Y.; Krylyuk, S.; Yoo, J.; Dayeh, S. A.; Davydov, A. V.; *et al. In Situ* Atomic-Scale Imaging of Electrochemical Lithiation in Silicon. *Nat. Nanotechnol.* **2012**, *7*, 749–756.
9. Liu, X. H.; Zhong, L.; Huang, S.; Mao, S. X.; Zhu, T.; Huang, J. Y. Size-Dependent Fracture of Silicon Nanoparticles during Lithiation. *ACS Nano* **2012**, *6*, 1522–1531.
10. Liu, N.; Wu, H.; Mcdowell, M. T.; Yao, Y.; Wang, C. M.; Cui, Y. A Yolk-Shell Design for Stabilized and Scalable Li-Ion Battery Alloy Anodes. *Nano Lett.* **2012**, *12*, 3315–3321.
11. Karki, K.; Epstein, E.; Cho, J. H.; Jia, Z.; Li, T.; Picraux, S. T.; Wang, C. S.; Cumings, J. Lithium-Assisted Electrochemical Welding in Silicon Nanowire Battery Electrodes. *Nano Lett.* **2012**, *12*, 1392–1397.
12. Mcdowell, M. T.; Ryu, I.; Lee, S. W.; Wang, C. M.; Nix, W. D.; Cui, Y. Studying the Kinetics of Crystalline Silicon Nanoparticle Lithiation with *In Situ* Transmission Electron Microscopy. *Adv. Mater.* **2012**, *24*, 6034–6041.
13. Liu, X. H.; Zheng, H.; Zhong, L.; Huan, S.; Karki, K.; Zhang, L. Q.; Liu, Y.; Kushima, A.; Liang, W. T.; Wang, J. W.; *et al.* Anisotropic Swelling and Fracture of Silicon Nanowires during Lithiation. *Nano Lett.* **2011**, *11*, 3312–3318.
14. Liu, X. H.; Huang, S.; Picraux, S. T.; Li, J.; Zhu, T.; Huang, J. Y. Reversible Nanopore Formation in Ge Nanowires during Lithiation−Delithiation Cycling: An *In Situ* Transmission Electron Microscopy Study. *Nano Lett.* **2011**, *11*, 3991–3997.
15. Liu, Y.; Hudak, N. S.; Huber, D. L.; Limmer, S. J.; Sullivan, J. P.; Huang, J. Y. *In Situ* Transmission Electron Microscopy Observation of Pulverization of Aluminum Nanowires and Evolution of the Thin Surface Al_2O_3 Layers during Lithiation−Delithiation Cycles. *Nano Lett.* **2011**, *11*, 4188–4194.
16. Liu, X. H.; Wang, J. W.; Liu, Y.; Zheng, H.; Kushima, A.; Huang, S.; Zhu, T.; Mao, S. X.; Li, J.; Zhang, S. L.; *et al. In Situ* Transmission Electron Microscopy of Electrochemical Lithiation, Delithiation and Deformation of Individual Graphene Nanoribbons. *Carbon* **2012**, *50*, 3836–3844.
17. Liu, Y.; Zheng, H.; Liu, X. H.; Huang, S.; Zhu, T.; Wang, J. W.; Kushima, A.; Hudak, N. S.; Huang, X.; Zhang, S. L.; *et al.* Lithiation-Induced Embrittlement of Multiwalled Carbon Nanotubes. *ACS Nano* **2011**, *5*, 7245–7253.
18. Kushima, A.; Liu, X. H.; Zhu, G.; Wang, Z. L.; Huang, J. Y.; Li, J. Leapfrog Cracking and Nanoamorphization of ZnO Nanowires during *In Situ* Electrochemical Lithiation. *Nano Lett.* **2011**, *11*, 4535–4541.
19. Liao, H. W.; Karki, K.; Zhang, Y.; Cumings, J.; Wang, Y. H. Interfacial Mechanics of Carbon Nanotube@Amorphous-Si Coaxial Nanostructures. *Adv. Mater.* **2011**, *23*, 4318–4322.
20. Wang, J. W.; Liu, X. H.; Zhao, K. J.; Palmer, A.; Patten, E.; Burton, D.; Mao, S. X.; Suo, Z. G.; Huang, J. Y. Sandwich-Lithiation and Longitudinal Crack in Amorphous Silicon Coated on Carbon Nanofibers. *ACS Nano* **2012**, *6*, 9158–9167.
21. Gu, M.; Li, Y.; Li, X. L.; Hu, S. Y.; Zhang, X. W.; Xu, W.; Thevuthasan, S.; Baer, D. R.; Zhang, J. G.; Liu, J.; *et al. In Situ* TEM Study of Lithiation Behavior of Silicon Nanoparticles Attached to and Embedded in a Carbon Matrix. *ACS Nano* **2012**, *6*, 8439–8447.
22. Ruzmetov, D.; Oleshko, V. P.; Haney, P. M.; Lezec, H. J.; Karki, K.; Baloch, K. H.; Agrawal, A. K.; Davydov, A. V.; Krylyuk, S.;

Liu, Y.; *et al.* Electrolyte Stability Determines Scaling Limits for Solid-State 3D Li Ion Batteries. *Nano Lett.* **2012**, *12*, 505–511.
23. Cabana, J.; Monconduit, L.; Larcher, D.; Palacin, M. R. Beyond Intercalation-Based Li-Ion Batteries: The State of the Art and Challenges of Electrode Materials Reacting through Conversion Reactions. *Adv. Mater.* **2010**, *22*, E170–E192.
24. Wang, X.; Tang, D. M.; Li, H. Q.; Yi, W.; Zhai, T. Y.; Bando, Y.; Golberg, D. Revealing the Conversion Mechanism of CuO Nanowires during Lithiation−Delithiation by *In Situ* Transmission Electron Microscopy. *Chem. Commun.* **2012**, *48*, 4812–4814.
25. Wang, F.; Yu, H. C.; Chen, M. H.; Wu, L.; Perieira, N.; Thorton, K.; Van Der Ven, A.; Zhu, Y.; Amatucci, G. G.; Graetz, J. Tracking Lithium Transport and Electrochemical Reactions in Nanoparticles. *Nat. Commun.* **2012**, *3*, 1201.
26. Balaya, P.; Li, H.; Kienle, L.; Maier, J. Fully Reversible Homogeneous and Heterogeneous Li Storage in RuO_2 with High Capacity. *Adv. Funct. Mater.* **2003**, *13*, 621–625.
27. Haynes, W. M. *CRC Handbook of Chemistry and Physics*; CRC Press: Boca Raton, FL, 2013; Vol. 93.
28. Delmer, O.; Balaya, P.; Kienle, L.; Maier, J. Enhanced Potential of Amorphous Electrode Materials: Case Study of RuO_2. *Adv. Mater.* **2008**, *20*, 501–505.
29. Balaya, P.; Bhattacharyya, A. J.; Jamnik, J.; Zhukovskii, Y. F.; Kotomin, E. A.; Maier, J. Nano-Ionics in the Context of Lithium Batteries. *J. Power Sources* **2006**, *159*, 171–178.
30. Delmer, O.; Maier, J. On the Chemical Potential of a Component in a Metastable Phase-Application to Li-Storage in the RuO_2-Li System. *Phys. Chem. Chem. Phys.* **2009**, *11*, 6424–6429.
31. Zhukovskii, Y. F.; Balaya, P.; Kotomin, E. A.; Maier, J. Evidence for Interfacial-Storage Anomaly in Nanocomposites for Lithium Batteries from First-Principles Simulations. *Phys. Rev. Lett.* **2006**, *96*, 058302.
32. Liu, Y. L.; Wu, Z. Y.; Lin, K. J.; Huang, J. J.; Chen, F. R.; Kai, J. J.; Lin, Y. H.; Jian, W. B.; Lin, J. J. Growth of Single-Crystalline RuO_2 Nanowires with One- and Two-Nanocontact Electrical Characterizations. *Appl. Phys. Lett.* **2007**, *90*, 013105.
33. Neupane, S.; Kaganas, G.; Valenzuela, R.; Kumari, L.; Wang, X. W.; Li, W. Z. Synthesis and Characterization of Ruthenium Dioxide Nanostructures. *J. Mater. Sci.* **2011**, *46*, 4803–4811.
34. Chen, C. C.; Chen, R. S.; Tsai, T. Y.; Huang, Y. S.; Tsai, D. S.; Tiong, K. K. The Growth and Characterization of Well Aligned RuO_2 Nanorods on Sapphire Substrates. *J. Phys.: Condens. Matter* **2004**, *16*, 8475–8484.
35. Liu, D. R.; Williams, D. B. The Electron-Energy-Loss Spectrum of Lithium Metal. *Philos. Mag. B* **1986**, *53*, L123–L128.
36. Wang, F.; Graetz, J.; Moreno, M. S.; Ma, C.; Wu, L. J.; Volkov, V.; Zhu, Y. M. Chemical Distribution and Bonding of Lithium in Intercalated Graphite: Identification with Optimized Electron Energy Loss Spectroscopy. *ACS Nano* **2011**, *5*, 1190–1197.
37. Mondio, G.; Neri, F.; Allegrini, M. Energy Loss Spectroscopy of RuO_2 Thin Films. *J. Appl. Phys.* **1997**, *82*, 1730–1735.
38. Zashkvar, V.; Redkin, V. S.; Korsunsk, M. Characteristic Electron Energy-Loss Spectrum for Ruthenium. *Fiz. Tverd. Tela* **1970**, *11*, 1944.
39. Kim, M. H.; Baik, J. M.; Lee, S. J.; Shin, H. Y.; Lee, J.; Yoon, S.; Stucky, G. D.; Moskovits, M.; Wodtke, A. M. Growth Direction Determination of a Single RuO_2 Nanowire by Polarized Raman Spectroscopy. *Appl. Phys. Lett.* **2010**, *96*, 213108.